Rates of Catalyzed Processes in Enzymes and Other Cooperative Media

Rates of Catalyzed Processes in Enzymes and Other Cooperative Media

Carlo Canepa[a]

(a) Dipartimento di Chimica Generale ed Organica Applicata, Università di Torino
Corso Massimo d'Azeglio 48, 10125 Torino, Italy
E-mail: carlo.canepa@unito.it

Abstract

Theoretical calculations on neutral model substrates of enzyme catalysis exhibit relatively high potential energy barriers with respect to values derived from experimental rate constants fitted to conventional expressions. A statistical theory based on the coupling of vibrational modes of the protein to the reaction coordinate affords a new expression for the unimolecular rate constant. Rate constants computed with the proposed theory are many orders of magnitude greater than the corresponding values given by traditional Arrhenius-type laws for a given potential energy barrier and temperature. Within this model, the hypothesis of a lowering of the potential energy barrier caused by specific interactions at the active site is no longer necessary. The dependence of the unimolecular rate constant by the energy barrier and temperature is given by the ratio of the incomplete and the complete gamma functions of Euler. The performance of the proposed model is tested against experimental rate constant for the hydrolysis of *N*-acetyl-*L*-tryptophan ethyl ester and *N*-acetyl-*L*-tyrosine ethyl ester catalyzed by α-chymotrypsin. The experimentally accessible quantity $(T/\beta)\partial_T \ln k$ may serve to discriminate between the conventional model (reduction of the potential energy barrier) and catalysis through dynamical coupling.

1. Introduction

Experimental rate constants for enzyme-catalyzed processes are usually fitted to Arrhenius-type equations affording energies of activation in the range of 42–50 *kJ mol*$^{-1}$.[1] On the other hand, various accurate theoretical calculations on model system at the active site fail to give barriers below ~84 *kJ mol*$^{-1}$, once the electroneutrality of the system is satisfied.[2] The effect of the medium, either explicitly modeled through the supermolecule approach, or approximated by polarized continuum models, does not significantly alter the gas-phase activation barriers. Recently, the role of protein dynamics in catalysis has become more evident and has been modeled by stochastic macromolecular mechanics,[3] QM/MM studies of tunneling,[4] and single-molecule approaches to conformational fluctuations.[5] Also, dynamical disorder theories take into account different channels to reaction products that originate from a distribution of potential energy barriers.[6] Each conformational change of the protein that occurs in the same time scale of the catalyzed process generates a reaction channel with its own rate constant. In this work the distribution of the reaction barrier due to conformational changes in the Michaelis-Menten complex is thought to be sharply peaked around the value $E^{\neq}$. Our computational experience with stereoelectronic effects on model systems related to enzyme-catalyzed reactions suggests that the influence of protein residues on the energy of reactant and transition structure is very similar, and does not significantly affect the reaction barrier. A stochastic treatment of a simple classical system embedded in a medium with cooperative modes led us to develop a model that predicts high reaction rates for the unimolecular rate constant of reactions exhibiting relatively high potential energy barriers for the breaking and forming of bonds between non-hydrogen atoms.[7] The expression for the unimolecular rate constant of the catalyzed step from the Michaelis-Menten complex to products is

$$k_a = \nu e^{-\beta E^{\neq}} \Omega_a , \qquad (1.1)$$

where ν represents the fundamental frequency with which a system with a number a of modes of the medium coupled to the reaction coordinate crosses the barrier, $E^{\neq}$ indicates the reaction potential energy barrier including the zero point energy (*ZPE*), and $\beta=(kT)^{-1}$. The enhancement exhibited by the rate constant in eq 1.1 with respect to a system without cooperative effects is given by the exponential sum function Ω_a

$$\Omega_a = \sum_{i=0}^{a-1} \frac{\left(\beta E^{\neq}\right)^i}{i!} . \qquad (1.2)$$

The sum 1.2 depends on the number of active modes *a* and the reduced barrier $\beta E^{\neq}$, and it can be as high as 1.4 10^{17}, a value experimentally observed for orotidine 5'-monophosphate decarboxylase.[8]

Low reaction barriers may be actually computed for systems (reagent and transition structure) bearing a whole charge. However, they follow from unrealistic gas-phase ion models, as can be shown by the explicit inclusion of the corresponding counterion. In fact, including a formate ion into the quantum-mechanical model for the N^1-protonated C4a-hydroperoxyflavin has a dramatic effect on the reaction barrier for oxygen atom transfer to dimethyl sulfide.[9] The isolated cation exhibits an artificially low MPW1K/6-31+G(*d,p*) barrier of 17.6 $kJ\ mol^{-1}$, while the corresponding barrier for the neutral ion pair is 66.8 $kJ\ mol^{-1}$, lower with respect to the unprotonated neutral system that reacts with a barrier of 90.5 $kJ\ mol^{-1}$. Thus, the charged system would appear to lower the barrier by 72.9 $kJ\ mol^{-1}$, with a corresponding increase in the rate constant of a factor of 6.18 10^{12}, while the actual reduction is 23.7 $kJ\ mol^{-1}$ with an increase in rate of only a factor of 1.46 10^4. This study aims to extend the rate law already proposed for enzyme-catalyzed processes and to show that eq 1.1 gives a correct description of experimental data. In this way the discrepancy between high experimental rate constants for enzyme-catalyzed reactions and the low rate constants computed with potential energy barriers obtained by quantum chemistry calculations on model systems is resolved. The proposed model for catalysis may be extended to other catalysts that operate through the binding of a substrate to a cavity, like zeolites[10] and cyclodextrins.[11] In section **3.1** we derive the rate law making use of an extended definition of a transition structure in phase space. Section **3.2** investigates the hydrolysis of *N*-acetyl-*L*-tryptophan ethyl ester and *N*-acetyl-*L*-tyrosine ethyl ester catalyzed by α-chymotrypsin both by fitting the experimental rate constants at different temperatures to eq 1.1 and by density functional theoretical calculations. Section **3.3** indicates the temperature dependence of the quantity $\lambda(T) = (T/\beta)\partial_T \ln k$ for the catalyzed process as a verification of the novel rate expression.

2. Methods of Calculation

Quantum chemistry calculations were carried out using the GAUSSIAN 98 suite of programs,[12] utilizing redundant internal coordinates geometry optimization.[13] All structures were fully optimized at the MPW1K[14] and B3LYP[15] levels of theory. The 6-31G(*d*) and 6-31+G(*d*,*p*) basis sets have been used throughout the study. Vibrational frequency calculations were used to characterize the stationary points as either minima or first-order saddle points at the level indicated. Solvation calculations were carried out with the isodensity surface polarized continuum model (IPCM) method.[16] Molecular graphics were obtained with the program Moldraw.[17] The thermodynamic potential *G* was evaluated at 298 *K* and 1 bar within the rigid rotor-harmonic oscillator approximation.[18]

3. Results and Discussion

3.1. Statistical Model for Enzymatic Activity.

We now derive an expression for the rate constant of a catalyzed reaction with potential energy barrier $E^{\neq}$, taking place in a system with total energy E and total number of vibrational modes s, of which a are strongly coupled to the reaction coordinate. We begin by extending the definition of transition structure to include the whole domain in phase space leading to product with a frequency $\nu(E)$. Following this extension we can write the energy-dependent rate constant as

$$\frac{d_t N}{N} = k\left(E, E^{\neq}\right) = \nu(E) \frac{\int_{H=\varepsilon}^{H=\varepsilon+d\varepsilon} dq_1 dp_1 \cdots dq_a dp_a / h^a \int_{H=E-\varepsilon-d\varepsilon}^{H=E-\varepsilon} dq_{a+1} dp_{a+1} \cdots dq_s dp_s / h^{s-a}}{\int_{H=E}^{H=E+dE} dq_1 dp_1 \cdots dq_s dp_s / h^s}$$

$$= \nu(E) \frac{\rho\left(E, E^{\neq}\right) dE}{\rho(E) dE} . \qquad (3.1.1)$$

Equation 3.1.1 represents the ratio between the number of vibrational states with energy $\varepsilon \geq E^{\neq}$ in a active modes, energy E-ε in s-a modes, and the total number of states. Once we have an explicit expression for $k(E,E^{\neq})$, we obtain the rate constant as the thermodynamic average

$$k_a(T) = \frac{1}{z_v}\int_{E^{\neq}}^{\infty} dE k\left(E, E^{\neq}\right)\rho(E)e^{-\beta E} = \frac{1}{z_v}\int_{E^{\neq}}^{\infty} dE\, \nu(E)\rho\left(E, E^{\neq}\right)e^{-\beta E}\ , \qquad (3.1.2)$$

where z_v is the vibrational partition function. Since eq 3.1.1 applies to the large composite system of substrate and medium, we neglect the translational and rotational contributions to the density of states. Assuming that the reactive frequency ν does not depend on E and changing the variable of integration to $x = \beta E$ we have

$$\frac{k_a(\bar{x})}{\nu} = \frac{1}{z_v}\int_{\bar{x}}^{\infty} dx\rho(x, \bar{x})e^{-x}\ , \qquad (3.1.3)$$

with $\bar{x} = \beta E^{\neq}$. Taking $\rho(E,E^{\neq})$ as the convolution integral between the density of states $\rho_a(\varepsilon)$ and $\rho_{s\text{-}a}(E\text{-}\varepsilon)$ we obtain

$$\rho\left(E, E^{\neq}\right) = \int_{E^{\neq}}^{E} d\varepsilon \rho_a(\varepsilon)\rho_{s-a}(E-\varepsilon)\,. \qquad (3.1.4)$$

We integrate eq 3.1.4 choosing the classical form for the vibrational density of states for $\rho_a(\varepsilon)$ and $\rho_{s\text{-}a}(E\text{-}\varepsilon)$,

$$\rho_n(E) = \frac{E^{n-1}}{\Gamma(n)}\prod_{i=1}^{n}\frac{1}{h\nu_i^{\neq}}\,. \qquad (3.1.5)$$

The density of vibrational states for the transition structure becomes

$$\rho(x,u) = \frac{\beta}{\Gamma(s)}x^{s-1}z_{\mathrm{v}}^{\neq}\psi_a(u), \qquad (3.1.6)$$

where $u = \bar{x}/x$ and

$$z_v^{\neq} = \prod_{i=1}^{s} \frac{kT}{h\nu_i^{\neq}}. \qquad (3.1.7)$$

The function $\psi_a(u) z_v^{\neq} / z_v$ thus represents the ratio between the volume in phase space that leads to products with frequency ν and the total volume which is associated with the reactant and compatible with the total energy *E*. The fundamental quantity $\psi_a(u)$ can be expressed in the following equivalent forms

$$\psi_a(u) = \sum_{i=0}^{a-1} \binom{s-1}{i} u^i (1-u)^{s-1-i}, \qquad (3.1.8a)$$

$$\psi_a(u) = 1 - \frac{\Gamma(s)}{\Gamma(a)} \sum_{i=0}^{s-1-a} \xi_i u^{a+i}, \qquad (3.1.8b)$$

and

$$\psi_a(u) = 1 - \frac{\mathrm{B}(a, s-a; u)}{\mathrm{B}(a, s-a)}. \qquad (3.1.8c)$$

In eq 3.1.8b

$$\xi_i = \frac{(-1)^i}{\Gamma(s-a-i)\Gamma(i+1)(a+i)}, \qquad (3.1.9)$$

and in eq 3.1.8c $\mathrm{B}(a, s-a; u)$ and $\mathrm{B}(a, s-a)$ are the incomplete ($\mathrm{B}(a,b;u) = \int_0^u dx\, x^{a-1}(1-x)^{b-1}$) and complete ($\mathrm{B}(a,b) = \int_0^1 dx\, x^{a-1}(1-x)^{b-1}$) beta functions, respectively. Plots of the function $\psi_a(u)$ are shown in Figure 1. For a relatively low number of active modes, the volume of phase space leading to products is already considerably large with respect to the volume computed by traditional theories ($\psi_1(u)$). Using eq 3.1.6 in 3.1.3, and assuming that the set $\{\nu_i^{\neq}\}$ does not depend on the energy, the rate constant takes the form

$$\frac{k_a(\bar{x})}{\nu} = \frac{z_v^{\neq}}{z_v}\frac{1}{\Gamma(s)}\int_{\bar{x}}^{\infty} dx\,\psi_a x^{s-1}e^{-x} \quad . \qquad (3.1.10)$$

The lower limit of the integral in eq 3.1.10 is given by the reduced energy barrier $\beta E^{\neq}$, since systems with total energy below this threshold do not contribute to the rate. The classical partition function z_v is given by

$$z_v = \prod_{i=1}^{s}\frac{kT}{h\nu_i}\frac{1}{\Gamma(s)}\int_0^{\infty} dx x^{s-1}e^{-x} = \prod_{i=1}^{s}\frac{kT}{h\nu_i}. \qquad (3.1.11)$$

Substituting eq 3.1.8a into 3.1.10 we obtain

$$\frac{k_a(\bar{x})}{\nu} = \frac{z_v^{\neq}}{z_v}\sum_{i=0}^{a-1}\frac{\bar{x}^i}{\Gamma(i+1)\Gamma(s-i)}\int_{\bar{x}}^{\infty} dx(x-\bar{x})^{s-1-i}e^{-x} \quad . \qquad (3.1.12)$$

and changing the variable of integration to $t = x - \bar{x}$ we have

$$\frac{k_a(\bar{x})}{\nu} = \frac{z_v^{\neq}}{z_v}e^{-\bar{x}}\sum_{i=0}^{a-1}\frac{\bar{x}^i}{i!}. \qquad (3.1.13)$$

Frequency contributions from the medium as well as from the reacting system are included in the set $\{\nu_i^{\neq}\}$ in eq 3.1.13. Also, the extended definition of the transition structure makes eq 3.1.13 dependent on the system-specific reactive frequency ν. From eqs 3.1.10 and 3.1.13 we recover the relation

$$\frac{1}{\Gamma(s)}\int_{\bar{x}}^{\infty} dx\,\psi_a x^{s-1}e^{-x} = e^{-\bar{x}}\sum_{i=0}^{a-1}\frac{\bar{x}^i}{i!}, \qquad (3.1.14)$$

already obtained in ref 7 for s and a integers using the form 3.1.8b for ψ_a. Since the right-hand side of eq 3.1.14 represents the survival function of the standard gamma distribution $x^{a-1}e^{-x}/\Gamma(a)$,[19] the function ψ_a has the property

$$\frac{1}{\Gamma(s)}\int_{\bar{x}}^{\infty} dx\,\psi_a x^{s-1}e^{-x} = \frac{1}{\Gamma(a)}\int_{\bar{x}}^{\infty} dx\,x^{a-1}e^{-x}\ . \qquad (3.1.15)$$

Equations 3.1.10 and 3.1.15 allow us to write the rate constant in the form

$$\frac{k_a(\bar{x})}{\nu} = \frac{z_v^{\neq}}{z_v}\frac{\Gamma(a,\bar{x})}{\Gamma(a)}, \qquad (3.1.16)$$

where $\Gamma(a) = \int_0^{\infty} dx\,x^{a-1}e^{-x}$ and $\Gamma(a,\bar{x}) = \int_{\bar{x}}^{\infty} dx\,x^{a-1}e^{-x}$ are the complete and incomplete gamma functions of Euler, respectively. The dependence of the rate constant from the potential energy barrier is thus in general not purely exponential, but it rather follows the incomplete gamma function. In the particular case of $a = 1$, the ratio $\Gamma(a,\bar{x})/\Gamma(a)$ in eq 3.1.16 is equal to $e^{-\bar{x}}$ and we recover the classical transition state theory with ν as the fundamental frequency. It must be emphasized that the vibrational partition functions pertain to the composite system of reactant and the surrounding medium, whether it is a catalyst or a solvent. The mechanisms operated by enzymes and other catalysts that couple their structures to the substrate differ from the corresponding processes in liquid solvents not in principle, but in the number of modes coupled to the reaction coordinate. For an arbitrary form of the density of vibrational states, eq 3.1.3 may be integrated iteratively by parts obtaining

$$\frac{k_a(\bar{x})}{\nu} = \frac{1}{z_v}\left(e^{-\bar{x}}\sum_{j=0}^{n}\left|\partial_{x^j}^{\,j}\rho(x,\bar{x})\right|_{\bar{x}} + \int_{\bar{x}}^{\infty} dx\,\partial_{x^{n+1}}^{\,n+1}\rho(x,\bar{x})e^{-x}\right), \qquad (3.1.17)$$

where $\partial_{x^n}^{\,n}$ indicates the derivative of order n with respect to x. Equation 3.1.17 may prompt further research in the density of vibrational states that does not follow the classical form 3.1.5.

Restricting the definition of a transition structure in phase space to a point in the proximity of a first-order saddle point with a momentum in the direction of products, we may recover a universal frequency in the expression for the rate constant. The average velocity in this direction is taken by a Maxwell-Boltzmann distribution with the integrals over the polar and azimuth angles restricted to one-half of their full range

$$\langle v \rangle = \int_0^{\pi} d\varphi \int_0^{\pi/2} d\theta \sin\theta \int_0^{\infty} dv \left(\frac{\beta\mu}{2\pi}\right)^{3/2} v^3 e^{-\beta\mu v^2/2} = \left(\frac{kT}{2\pi\mu}\right)^{1/2}. \qquad (3.1.18)$$

The ratio of <*v*> over the de Broglie wavelength $\lambda = h/(2\pi\mu kT)^{1/2}$ gives the fundamental frequency

$$\nu = \frac{\langle v \rangle}{\lambda} = \frac{kT}{h}. \qquad (3.1.19)$$

3.2. Performance of the Model.

Experimental data for the hydrolysis of *N*-acetyl-*L*-tryptophan ethyl ester and *N*-acetyl-*L*-tyrosine ethyl ester catalyzed by *α*-chymotrypsin[20] were fitted to eq 1.1. Couples of values for *v* and $E^{\neq}$, obtained for each value of *a*, and standard deviations to the *n* experimental points $\bar{k}(T_i)$

$$\sigma = \sqrt{\frac{1}{n}\sum_{i=1}^{n}\left[k_a(T_i) - \bar{k}(T_i)\right]^2} \qquad (3.2.1)$$

for each fit are listed in Tables 1 and 2. The ratio between σ and the average rate constant in the temperature range of the experiment is on the order of 10^{-2}, indicating that the regressions in Tables 1 and 2 represent good fits to experimental data. The best fits (minimum σ) are given by 34 and 1 oscillators for *N*-acetyl-*L*-tryptophan ethyl ester and *N*-acetyl-*L*-tyrosine ethyl ester, respectively. Clearly, the values of *v* and $E^{\neq}$ given by the best fits in Tables 1 and 2, so different for similar reactions catalyzed by the same enzyme, are not consistent and a choice must be made between the two different sets.

To this purpose, density functional calculations were performed on model substrates to determine the potential energy barrier for hydrolysis. As a reference point we take the uncatalyzed hydrolysis of methyl acetate that proceeds with the MPW1K/6-31G(*d*) potential and free energy barriers of 104.9 and 121.7 *kJ mol*$^{-1}$ (Figure 2). As a consequence of the similarity in the structural and electronic features of methyl and ethyl acetate, both esters are expected to exhibit similar reaction barriers for hydrolysis. In fact, the calculated free energy barrier for the hydrolysis of methyl acetate is in good agreement with the experimental value of 127.9 *kJ mol*$^{-1}$ for the hydrolysis of ethyl acetate.[21] Since TS-**2** exhibits a proton relay from the nucleophile water molecule toward the carbonyl oxygen, all structures have been optimized using the MPW1K functional of Truhlar,[11]

especially designed for hydrogen transfer reactions. All structures were also re-optimized with the more established B3LYP functional of Becke. In all cases the difference between potential and free energy barriers computed with the two methods was found to be minimal (Table 3). The extended organization of the water molecules in TS-**2** is responsible for the high entropy of activation that reflects in the 16.8 *kJ mol*$^{-1}$ difference between $\Delta G^{\neq}$ and $\Delta E^{\neq}_{ZPE}$ (potential energy barrier including the zero point energy). The reaction path from TS-**2** to product was followed by an intrinsic reaction coordinate (IRC) calculation[22] affording the reaction intermediate $CH_3C(OH)_2OCH_3 \bullet H_2O$, already observed by Schmeer[23] for the hydrolysis of ethyl acetate. The effect of the basis set on the reaction barrier was determined re-optimizing minimum **1** and TS-**2** at the MPW1K/6-31+G(*d,p*) level. The $\Delta E^{\neq}_{ZPE}$ and $\Delta G^{\neq}$ resulted in 115.4 and 133.0 *kJ mol*$^{-1}$, respectively, indicating that the 6-31G(*d*) basis set gives an adequate description of the relative energetics of the species involved.

In the first step of hydrolyses catalyzed by α-chymotrypsin, the amino acid Ser-195 is the attacking nucleophile at the carbonyl group of the ester. His-57 assists the attack by hydrogen bonding to the hydroxyl group of serine, its effect enhanced by the interaction of the imidazole ring with Asp-102. We model this series of interactions with the participation of an imidazole ring as a general base catalyst favoring the attack of a water molecule to the carbonyl. Formic acid further assists with a hydrogen bond to the imidazole ring or the carbonyl group of the ester, depending on its ionization state. We first modeled the hydrogen bond between Asp-102 and His-57[24] by a formate anion binding to the hydrogen atom of the imidazole ring (structure **3**, Figure 3). Although we advocate the opportunity of extending the model until all counterions are accounted for and ensure electroneutrality of the system, we chose to investigate first a smaller portion of the microenvironment around the substrate with –1*e* charge. The counterion relative to the formate-imidazole anion has thus been omitted in structure **3** and TS-**4**. The resulting potential energy barrier for the first step of hydrolysis is 94.2 *kJ mol*$^{-1}$.[25] The calculated barrier is lowered to 81.0 *kJ mol*$^{-1}$ in TS-**6**, where formic acid is in its neutral state. The two models are thought to represent the catalytic steps of α-chymotrypsin at basic and acidic *pH*, respectively.[26] However, both barriers are significantly above the range predicted by conventional Arrhenius analysis. This behavior has already been observed with other model systems;[2,7,9] the interaction of the substrate with the coenzyme and the active site is responsible for a considerable reduction of the potential energy barrier with respect to the gas phase or solvated process. Nevertheless, the resulting barriers are still significantly above the expected range of 42–50 *kJ mol*$^{-1}$. The effect of solvation was also estimated through single-point calculations at the MPW1K/6-31G(*d*) level on minimum **5** and TS-**6** within the IPCM model with the upper bound value of 6 for the relative permittivity of the protein.[27] The

potential energy barrier (84.0 *kJ mol*$^{-1}$) is close to the gas-phase value and reflects the small effect of the relatively hydrophobic medium on the reaction barrier of polar substrates.

To assess the energy barriers for hydrolysis of the actual enzyme substrates *N*-acetyl-*L*-tryptophan ethyl ester and *N*-acetyl-*L*-tyrosine ethyl ester, the structures of clusters of the substrates with two water molecules (**7** and **9**) and the corresponding transition structures for the attack to the carbonyl (TS-**8** and TS-**10**) were optimized at the MPW1K/6-31G(*d*) level of theory (Figures 4 and 5). The potential energy barrier for hydrolysis of *N*-acetyl-*L*-tryptophan ethyl ester and *N*-acetyl-*L*-tyrosine ethyl ester are 128.0 and 110.3 *kJ mol*$^{-1}$, respectively. Re-optimization at the B3LYP/6-31G(*d*) level does not significantly affect these results (Table 3). The reaction barrier for the nucleophilic attack of a water molecule on *N*-acetyl-*L*-tyrosine ethyl ester parallels the corresponding energetics of methyl acetate. The uncatalyzed hydrolysis of *N*-acetyl-*L*-tryptophan ethyl ester is predicted to be slower. Two typical regressions of experimental rate constants at different temperatures to eq 1.1 are shown in Figure 6. The potential energy barriers obtained by the theoretical calculations are in the range corresponding to 15-20 active modes. Conversely, the conventional regression to the Rice-Ramsperger-Kassel (RRK) expression[28] gives 50.9 and 45.7 *kJ mol*$^{-1}$ as potential energy barriers for the catalyzed hydrolysis of *N*-acetyl-*L*-tryptophan ethyl ester and *N*-acetyl-*L*-tyrosine ethyl ester, respectively.[29]

3.3. Relationship with Transition State Theory.

The conventional theory of rates is expressed by eq 3.1.13 with $a = 1$ and eq 3.1.19 as the fundamental frequency. Catalysis is consequently interpreted as a lowering of the potential energy barrier $E^{\neq}$ in the expression for the rate constant

$$k_1 = \frac{kT}{h}\frac{z_v^{\neq}}{z_v} e^{-\beta E^{\neq}} . \qquad (3.3.1)$$

Applying the operator $(T/\beta)\partial_T \, ln$ on both sides of eq 3.3.1, we obtain the quantity

$$\lambda_1(T) = \frac{T}{\beta}\partial_T \, ln k_1 = \frac{1}{\beta} + \Delta u^{\neq}(T) + E^{\neq} , \qquad (3.3.2)$$

that depends on temperature through the terms $1/\beta$ and the difference of thermal corrections ($\Delta u^{\neq}$) to the potential energy of the transition structure and reagent.

The same operation performed on eq 3.1.13 affords the quantity $\lambda_a(T)$

$$\lambda_a(T) = \frac{T}{\beta}\partial_T \ln k_a = \Delta u^{\neq}(T) + E_a^{\neq}\frac{\Delta\Omega_a}{\Omega_a}, \qquad (3.3.3)$$

where $\partial_x = \partial/\partial x$, $\Delta\Omega_a = \Omega_a - \Omega_{a-1} = \left(\beta E_a^{\neq}\right)^{a-1}/\Gamma(a)$, and a is the number of active modes. In eq 3.3.3 the dependence on temperature is more pronounced, being given by both terms $\Delta u^{\neq}$ and $\Delta\Omega_a/\Omega_a$. Plots of $\lambda_1(T)$ and $\lambda_a(T)$, with $\Delta u^{\neq}$ calculated at different temperatures for minimum **7** and TS-**8** (hydrolysis of *N*-acetyl-*L*-tryptophan ethyl ester), are shown in Figure 7. The behavior of $\lambda(T)$ may determine if the cooperative mechanism of coupled active modes to the reaction coordinate is in effect. Indeed, increased enthalpies of activation at reduced temperatures (biphasic Arrhenius behavior) have already been observed in thermophilic enzymes,[30] with the experimental values for $\Delta H^{\neq}$ of 98.7 and 61.1 $kJ\ mol^{-1}$ in the 5-30 and 30-65 ^oC temperature ranges, respectively. The plots in Figure 7 exhibit this kind of behavior, more pronounced for high values of a.

4. Conclusions

1. This work relates a new rate expression for enzyme-catalyzed processes to conventional transition state theory. In the above formulation the potential energy barrier of a process is regarded as an intrinsic property that is not significantly affected by the environment. The dramatic increase in rate of enzymatic processes is interpreted as a consequence of the dynamic coupling between modes of the medium to the reaction coordinate.

2. In general, unimolecular rate constants for enzyme-catalyzed reactions depend on the reduced barrier $\beta E^{\neq}$ as the incomplete gamma function of Euler (eq 3.1.16). This law reduces to the exponential dependence of conventional transition state theory in the particular case of one active mode. The quantity $\lambda(T) = (T/\beta)\partial_T \ln k$, evaluated experimentally at different temperatures for the catalyzed process, is proposed as a test to support or disprove the theory.

3. The performance of the proposed rate expression was tested against experimental rate constants for the hydrolysis of *N*-acetyl-*L*-tryptophan ethyl ester and *N*-acetyl-*L*-tyrosine ethyl ester catalyzed by α-chymotrypsin. The potential energy barriers computed by density functional theory for the same processes were found to be considerably higher with respect to the values predicted by an Arrhenius analysis. Using the potential energy barriers obtained by theoretical calculations, the

proposed rate expression affords the experimental unimolecular rate constants for ~15 active modes of α-chymotrypsin.

5. Summary

The expression for the unimolecular rate constant for enzyme-catalyzed processes reported in a previous work is re-derived more generally. While the traditional transition state theory explains catalysis in terms of reduced barriers, the above result regards reaction barriers as intrinsic properties. The considerable rate enhancements exhibited by enzyme-catalyzed reactions with respect to the corresponding processes in solution are interpreted as a consequence of the enhanced coupling of active modes to the reaction coordinate. Density functional calculations give potential energy barriers for the hydrolysis of two enzyme substrates in excess of values predicted by the Arrhenius analysis of experimental data. The novel rate expression reported in this work is able to account for high rates without resorting to a reduction in the reaction barrier which is not supported by theoretical calculations.

Acknowledgement

The author is grateful to Profs. Paolo Cermelli and Piero Ugliengo for helpful discussions.

Figure 1. Plots of the quantity ψ_{10} (solid line) and ψ_{30} (dotted line) for s = 100. The corresponding function for one active mode (ψ_1, dashed line) is also shown for comparison.

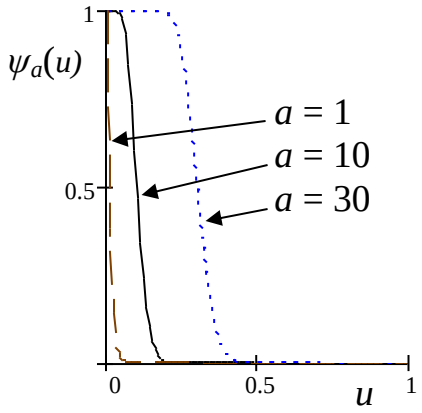

Figure 2. Potential energy ($\Delta E^{\neq}_{ZPE}$) and free energy ($\Delta G^{\neq}$) of activation for the uncatalyzed hydrolysis of methyl acetate. Geometries are optimized at the MPW1K/6-31G(*d*) level; distances are in angstroms. Values at the B3LYP/6-31G(*d*) level of theory are reported in parentheses.

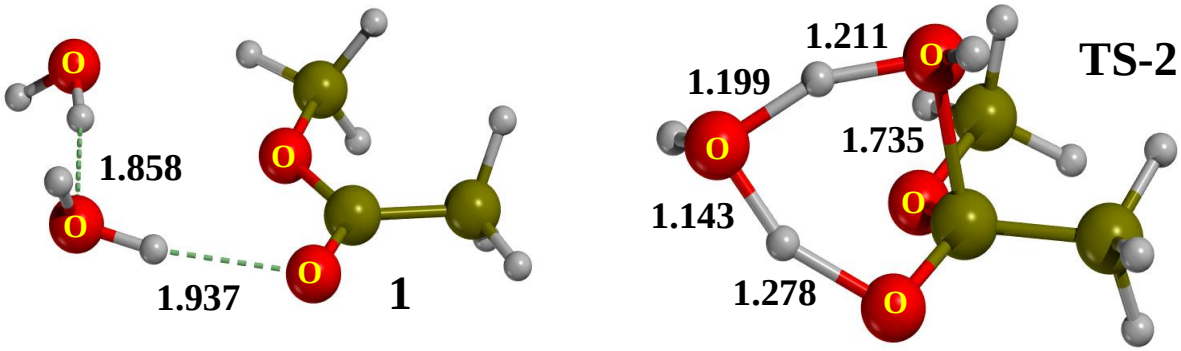

$\Delta E^{\neq}_{ZPE}$ = 104.9 (106.8) *kJ mol*$^{-1}$

$\Delta G^{\neq}$ = 121.7 (123.2) *kJ mol*$^{-1}$

Figure 3. Potential energies ($\Delta E^{\neq}_{ZPE}$) and free energies ($\Delta G^{\neq}$) of activation for the hydrolysis of methyl acetate catalyzed by imidazole hydrogen bonded to a formate anion (**3** and TS-**4**) and formic acid (**5** and TS-**6**). Geometries are optimized at the MPW1K/6-31G(*d*) level; distances are in angstroms. Values at the B3LYP/6-31G(*d*) level of theory are reported in parentheses.

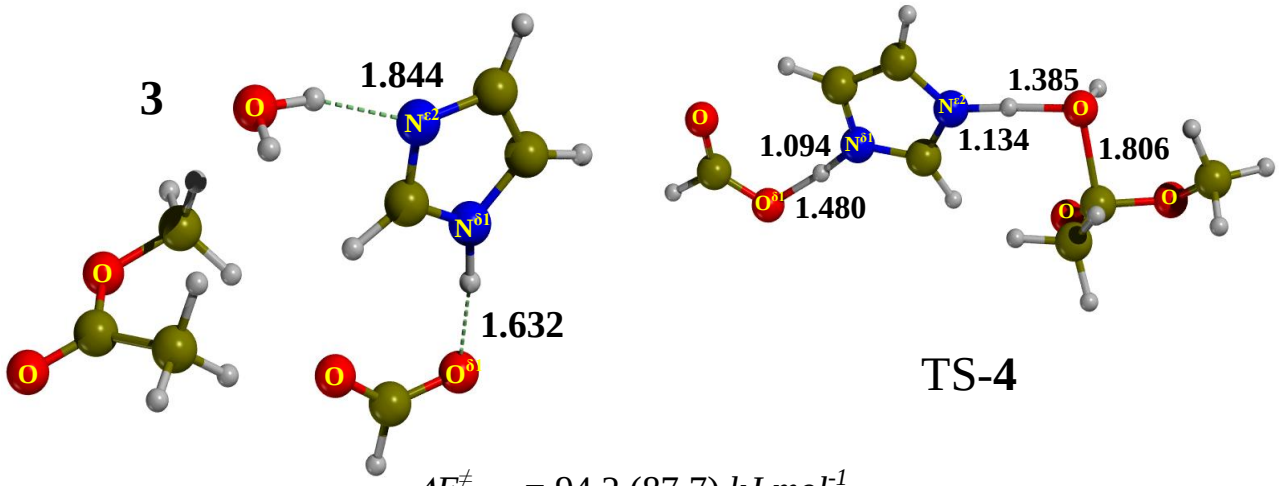

$\Delta E^{\neq}_{ZPE}$ = 94.2 (87.7) *kJ mol*$^{-1}$

$\Delta G^{\neq}$ = 108.3 (101.7) *kJ mol*$^{-1}$

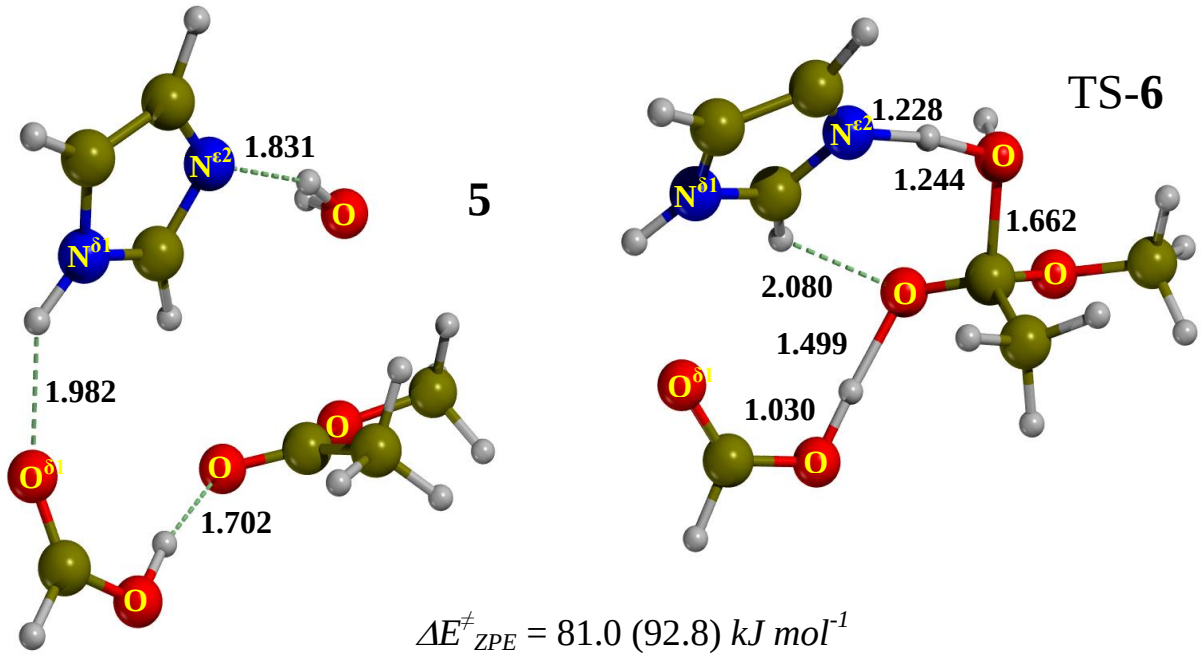

$\Delta E^{\neq}_{ZPE}$ = 81.0 (92.8) *kJ mol*$^{-1}$

$\Delta G^{\neq}$ = 96.9 (108.2) *kJ mol*$^{-1}$

Figure 4. Relative energy ($\Delta E^{\neq}_{ZPE}$) and free energy ($\Delta G^{\neq}$) of reactant model *N*-acetyl-*L*-tryptophan ethyl ester (**7**) and the transition structure for hydrolysis (TS-**8**). Geometries are optimized at the MPW1K/6-31G(*d*) level; distances are in angstroms. Values at the B3LYP/6-31G(*d*) level of theory are reported in parentheses.

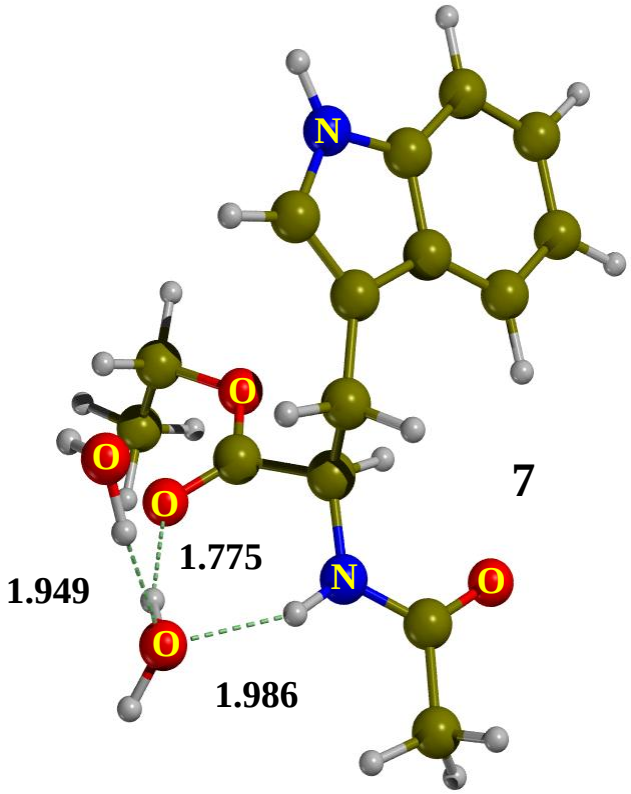

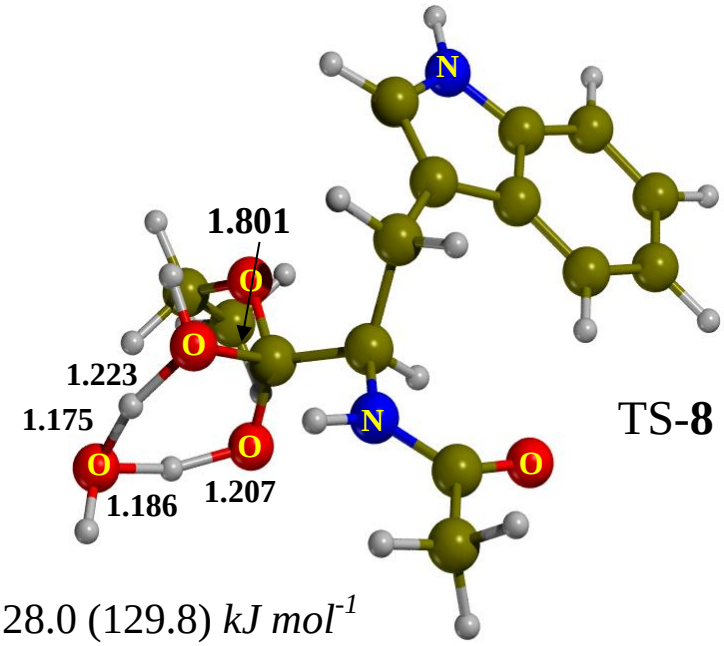

$\Delta E^{\neq}_{ZPE}$ = 128.0 (129.8) *kJ mol*$^{-1}$

$\Delta G^{\neq}$ = 141.0 (140.0) *kJ mol*$^{-1}$

Figure 5. Relative energy ($\Delta E^{\neq}_{ZPE}$) and free energy ($\Delta G^{\neq}$) of reactant model *N*-acetyl-*L*-tyrosine ethyl ester (**9**) and the transition structure for hydrolysis (TS-**10**). Geometries are optimized at the MPW1K/6-31G(*d*) level; distances are in angstroms. Values at the B3LYP/6-31G(*d*) level of theory are reported in parentheses.

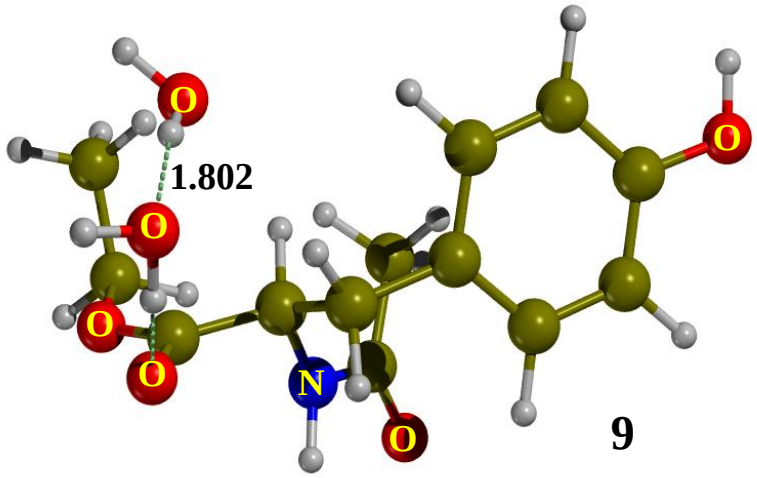

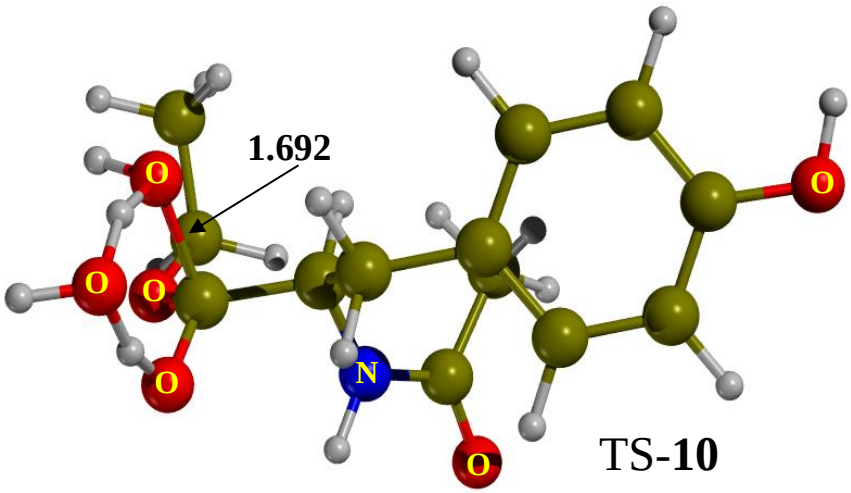

$\Delta E^{\neq}_{ZPE}$ = 110.3 (114.1) *kJ mol*$^{-1}$

$\Delta G^{\neq}$ = 118.5 (122.3) *kJ mol*$^{-1}$

Figure 6. Regressions of the experimental rate constants for hydrolysis of *N*-acetyl-*L*-tryptophan ethyl ester (**1**) and *N*-acetyl-*L*-tyrosine ethyl ester (**2**) catalyzed by *α*-chymotrypsin. The dots represent experimental points and the curves eq 1.1 for the specified values of *a* (coupled modes to the reaction coordinate) and $E^{\neq}$ (potential energy barrier, *kJ mol*$^{-1}$). The conventional theory predicts barriers of 50.9 and 45.7 *kJ mol*$^{-1}$ for the hydrolysis of **1** and **2**, respectively.

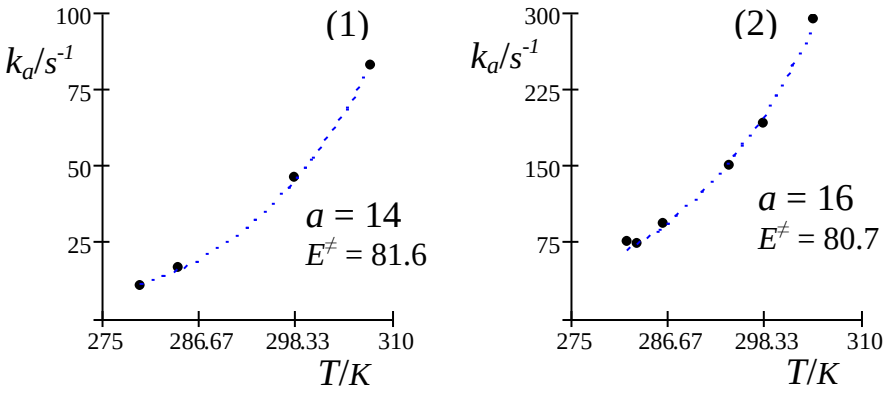

Figure 7. Predicted dependence on temperature of the quantities $\lambda_a(T)$ (**1**, **2**, and **3**) and $\lambda_1(T)$ (**4**), computed for the catalyzed hydrolysis of *N*-acetyl-*L*-tryptophan ethyl ester with the specified values of *a* (coupled modes to the reaction coordinate) and $E_a^{\neq}$ (potential energy barrier).

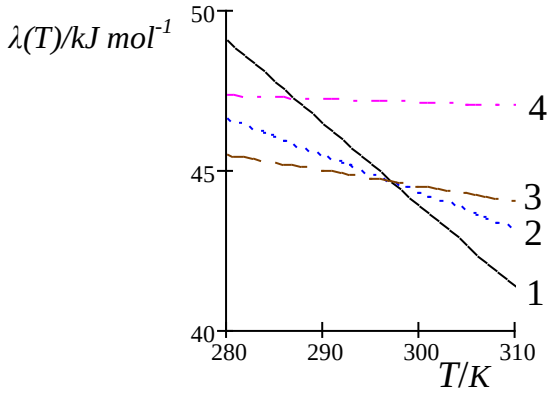

(1) a = 34, $E_a^{\neq} = 128.9\,kJ\,mol^{-1}$

(2) a = 14, $E_a^{\neq} = 81.6\,kJ\,mol^{-1}$

(3) a = 5, $E_a^{\neq} = 60.3\,kJ\,mol^{-1}$

(4) The conventional theory affords the nearly constant $\lambda_1 = 1/\beta + \Delta u^{\neq}(T) + 50.9\,kJ\,mol^{-1}$.

Table 1: Parameters relative to equation 1.1 for the hydrolysis of *N*-acetyl-*L*-tryptophan ethyl ester (**7**) catalyzed by α-chymotrypsin.

a	ν/s^{-1}	$\Delta E^{\neq}/kJ\ mol^{-1}$	σ/s^{-1}
1	$3.79\ 10^{10}$	50.9	0.521
5	$9.84\ 10^{7}$	60.3	0.480
10	$3.41\ 10^{6}$	72.1	0.432
15	$4.74\ 10^{5}$	84.0	0.390
20	$1.26\ 10^{5}$	95.8	0.355
25	$4.79\ 10^{4}$	107.6	0.329
30	$2.29\ 10^{4}$	119.5	0.314
34*	$1.42\ 10^{4}$	128.9	0.310
35	$1.28\ 10^{4}$	131.3	0.311
40	$7.99\ 10^{3}$	143.1	0.319
45	$5.40\ 10^{3}$	155.0	0.338
50	$3.88\ 10^{3}$	166.9	0.366
55	$2.92\ 10^{3}$	178.7	0.399
60	$2.29\ 10^{3}$	190.6	0.438
65	$1.85\ 10^{3}$	202.5	0.480
70	$1.53\ 10^{3}$	214.3	0.525
75	$1.29\ 10^{3}$	226.2	0.571
80	$1.11\ 10^{3}$	238.1	0.619

(*) Value of a that minimizes σ

Table 2: Parameters relative to equation 1.1 for the hydrolysis of *N*-acetyl-*L*-tyrosine ethyl ester (**9**) catalyzed by α-chymotrypsin.

a	ν/s^{-1}	$\Delta E^{\neq}/kJ\ mol^{-1}$	σ/s^{-1}
1*	$2.05\ 10^{10}$	45.7	5.181
5	$7.23\ 10^{7}$	55.0	5.328
10	$3.27\ 10^{6}$	66.7	5.509
15	$5.51\ 10^{5}$	78.4	5.688
20	$1.68\ 10^{5}$	90.1	5.865
25	$7.15\ 10^{4}$	101.8	6.040
30	$3.74\ 10^{4}$	113.5	6.212
35	$2.25\ 10^{4}$	125.2	6.383
40	$1.49\ 10^{4}$	136.9	6.552
45	$1.06\ 10^{4}$	148.6	6.720
50	$7.93\ 10^{3}$	160.4	6.885
55	$6.20\ 10^{3}$	172.1	7.050
60	$5.02\ 10^{3}$	183.8	7.212
65	$4.17\ 10^{3}$	195.6	7.373
70	$3.54\ 10^{3}$	207.3	7.533
75	$3.06\ 10^{3}$	219.1	7.692
80	$2.68\ 10^{3}$	230.8	7.849

(*) Value of a that minimizes σ

Table 3: Reaction barriers ($\Delta E^{\neq}$/*kJ mol*$^{-1}$) and activation Gibbs free energies at 298 *K* ($\Delta G^{\neq}$/*kJ mol*$^{-1}$) based upon MPW1K/6-31G(*d*) and B3LYP/6-31G(*d*) calculations for the hydrolysis reactions represented in Figures 2-5.

Process	*MPW1K*		*B3LYP*	
	$\Delta E^{\neq}$	$\Delta G^{\neq}$	$\Delta E^{\neq}$	$\Delta G^{\neq}$
1 → TS-2	104.9	121.7	106.8	123.2
3 → TS-4	94.2	108.6	87.7	101.7
5 → TS-6	81.0	96.9	92.8	108.2
7 → TS-8	128.0	141.0	129.7	140.0
9 → TS-10	110.2	118.4	114.1	122.3

References and Notes

[1] *(a)* Wolfenden, R.; Snider, M. J. *Acc. Chem. Res*. **2001**, *34*, 938. *(b)* Wolfenden, R.; Snider, M.; Ridgway, C.; Miller, B. *J. Am. Chem. Soc*. **1999**, *121*, 7419.

[2] *(a)* Bach, R. D.; Canepa, C. *J. Am. Chem. Soc*. **1997**, *119*, 11725. *(b)* Bach, R. D.; Canepa, C.; Glukhovtsev, M. N. *J. Am. Chem. Soc*. **1999**, *121*, 6542.

[3] Quian, H. *J. Phys. Chem. B* **2002**, *106*, 2065.

[4] Faulder, P. F.; Tresadern, G.; Chohan, K. K.; Scrutton, N. S.; Sutcliffe, M. J.; Hillier, I. H.; Burton, N. A. *J. Am. Chem. Soc*. **2001**, *123*, 8604.

[5] Sunney Xie, X. *J. Chem. Phys*. **2002**, *117*, 11024.

[6] Vlad, M. O.; Ross, J.; Huber, D. L. *J. Phys. Chem. B* **1999**, *103*, 1563.

[7] Canepa, C.; Bach, R. D. *Phys. Chem. Chem. Phys*. **2001**, *3*, 4072.

[8] Radzicka A.; Wolfenden, R. *Science* **1995**, *267*, 90.

[9] Canepa, C.; Bach, R. D.; Dmitrenko, O. *J. Org. Chem.* **2002**, *67*, 8653.

[10] *(a)* Corma, A. *Chem. Rev*. **1997**, *97*, 2373. *(b)* Demontis, P.; Suffritti, G. B. *Chem. Rev*. **1997**, *97*, 2845.

[11] Easton, C. J.; Lincoln, S. F. In *Modified Cyclodextrins*; Imperial College Press: London, 1999.

[12] Gaussian98, Frisch, M. J.; Trucks, G. W.; Schlegel, H. B.; Scuseria, G. E.; Robb, M. A.; Cheeseman, J. R.; Zakrzewski, V. G.; Montgomery, J. A. Jr.; Stratmann, R. E.; Burant, J. C.; Dapprich, S.; Millam, J. M.; Daniels, A. D.; Kudin, K. N.; Strain, M. C.; Farkas, O.; Tomasi, J.; Barone, V.; Cossi, M.; Cammi, R.; Mennucci, B.; Pomelli, C.; Adamo, C.; Clifford, S.; Ochterski, J.; Petersson, G. A.; Ayala, P. Y.; Cui, Q.; Morokuma, K.; Malick, D. K.; Rabuck, A. D.; Raghavachari, K.; Foresman, J. B.; Cioslowski, J.; Ortiz, J. V.; Baboul, A. G.; Stefanov, B. B.; Liu, G.; Liashenko, A.; Piskorz, P.; Komaromi, I.; Gomperts, R.; Martin, R. L.; Fox, D. J.; Keith, T.; Al-Laham, M. A.; Peng, C. Y.; Nanayakkara, A.; Gonzalez, C.; Challacombe, M.; Gill, P. M. W.; Johnson, B.; Chen, W.; Wong, M. W.; Andres, J. L.; Gonzalez, C.; Head-Gordon, M.; Replogle, E. S.; Pople, J. A. Gaussian98, Inc.:, Pittsburgh, PA, 1998.

[13] Peng, C.; Ayala, P. Y.; Schlegel, H. B.; Frisch, M. J. *J. Comput. Chem.* **1996**, *17*, 49.

[14] *(a)* Lynch, B. J.; Fast, P. L.; Harris, M.; Truhlar, D. G. *J. Phys. Chem. A* **2000**, *104*, 4811. *(b)* Lynch, B. J.; Truhlar, D. G. *J. Phys. Chem. A* **2001**, *105*, 2936.

[15] *(a)* Becke, A. D. *J. Chem. Phys*. **1993**, *98*, 5648. *(b)* Stevens, P. J.; Devlin, F. J.; Chablowski, C. F.; Frisch, M. J. *J. Phys. Chem*. **1994**, *80*, 11623.

[16] Foresman, J. B.; Keith, T. A.; Wiberg, K. B.; Snoonian, J.; Frisch, M. J. *J. Phys. Chem.* **1996**, *100*, 16098.

[17] *(a)* Ugliengo, P.; Viterbo, D.; Borzani, G. *J. Appl. Crystallogr*. **1988**, *21*, 75. *(b)* Ugliengo, P.; Borzani, G.; Viterbo, D. *Z. Crystallogr*. **1988**, *185*, 712. *(c)* Ugliengo, P.; Viterbo, D.; Chiari, G. *Z. Crystallogr*. **1993**, *207*, 9.

[18] McQuarrie, D. A. In *Statistical Thermodynamics*; University Science Books: Mill Valley, CA, 1973.

[19] Råde, L.; Westergren, B. In *Mathematics Handbook*; CRC Press: Boca Raton, 1990.

[20] Bender, M. L.; Kézdy, F. J.; Gunter, C. R. *J. Am. Chem. Soc*. **1964**, *86*, 3714.

[21] Skrabal, A.; Zahorca, A. *Monatsh. Chem.* **1929**, *54*, 562.

[22] *(a)* Gonzalez, C.; Schlegel, H. B. *J. Chem. Phys*. **1989**, *90*, 2154. *(b)* Gonzalez, C.; Schlegel, H. B. *J. Phys. Chem.* **1990**, *94*, 5523.

[23] Schmeer, G.; Sturm, P. *Phys. Chem. Chem. Phys*. **1999**, *1*, 1025.

[24] The exact nature of the hydrogen bond between the $N^{\delta 1}$ of His-57 and the $O^{\delta 1}$ of Asp-102 is still controversial. See Westler, W. M.; Frey, P. A.; Lin, J.; Wemmer, D. E.; Morimoto, H.; Williams, P. G.; Markley, J. L. *J. Am. Chem. Soc*. **2002**, *124*, 4196 and references therein.

[25] An IRC calculation shows that TS-**4** is not directly connected to the tetrahedral intermediate $CH_3C(OH)_2OCH_3 \bullet C_3N_2H_4 \bullet HCOO^{(-)}$ on the MPW1K/6-31G(*d*) potential energy surface. There is a further minimum between the two species, 92.7 *kJ mol*$^{-1}$ from the reactant cluster. In this structure the $N^{\epsilon 2}$ proton is hydrogen bonded both to the incoming oxygen nucleophile and the carbonyl oxygen. This minimum is connected to a transition structure at 92.9 *kJ mol*$^{-1}$ that in turn leads to the tetrahedral intermediate. These topological features have no consequence on the thermal-averaged properties of the system.

[26] Ash, E. L.; Sudmeier, J. L.; De Fabo, E. C.; Bachovchin, W. W. *Science* **1997**, *278*, 1128.

[27] Takashima, S. *J. Chem. Phys*. **1996**, *100*, 3855.

[28] The high-pressure limit of the RRK expression has the same form as the Arrhenius equation for a unimolecular reaction, but the preexponential factor and the energy of activation have a definite physical meaning. The RRK theory is recovered from eq 1.1 in the particular case of one active mode. For a discussion of RRK theory, see: Steinfeld, J. I.; Francisco, J. S.; Hase, W. L. In *Chemical Kinetics and Dynamics*; Prentice Hall: Englewood Cliffs, NJ, 1989.

[29] The corresponding activation enthalpies for the deacylation step of α-chymotrypsin reported in ref 20 are 50.2 *kJ mol*$^{-1}$ for *N*-acetyl-*L*-tryptophan ethyl ester and 43.1 *kJ mol*$^{-1}$ for *N*-acetyl-*L*-tyrosine ethyl ester.

[30] Kohen, A.; Cannio, R.; Bartolucci, S.; Klinman, J. P. *Nature* **1999**, *399*, 496.